Original Article

Comparative characterization of osteoclasts derived from murine bone marrow macrophages and RAW 264.7 cells using quantitative proteomics†

Andrew Y.H. Ng[1,2,4, a,b,c], Chengjian Tu, Ph.D.[3,4], Shichen Shen, Ph.D.[3,4], Ding Xu, Ph.D.[2], Merry Jo Oursler, Ph.D.[5], Jun Qu, Ph.D.[3,4]*, Shuying Yang, M.D., Ph.D.[1,a,b,]*

[1] Department of Anatomy and Cell Biology, School of Dental Medicine, University of Pennsylvania, Philadelphia, PA

[2] Department of Oral Biology, School of Dental Medicine, University at Buffalo, Buffalo, NY

[3] Department of Pharmaceutical Science, School of Pharmacy and Pharmaceutical Sciences, University at Buffalo, NY

[4] New York State Center of Excellence in Bioinformatics and Life Sciences, Buffalo, NY

[5] Department of Medicine, Endocrine Research Unit, Mayo Clinic, Rochester, MN

[a] National Institute of Arthritis and Musculoskeletal and Skin Diseases (NIAMS)

[b] National Institute of Aging (NIA)

[c] Mark Diamond Research Fund (MDRF)

Additional Supporting Information may be found in the online version of this article

Initial Date Submitted March 5, 2018; Date Revision Submitted April 26, 2018; Date Final Disposition Set May 7, 2018

JBMR Plus

DOI 10.1002/jbm4.10058

*Corresponding authors:

Shuying Yang, M.D., Ph.D.
Associate Professor
University of Pennsylvania
Department of Anatomy and Cell Biology
Levy 443, 240 S. 40th St
Philadelphia, PA 19104
Phone: (215) 898-2685
Email: shuyingy@upenn.edu

Jun Qu, Ph.D.
Associate Professor
University at Buffalo
Department of Pharmaceutical Sciences
B3-302, 701 Ellicott St.
Buffalo, NY 14203
Phone: (716) 881-7513
Email: junqu@buffalo.edu

ABSTRACT

Osteoclasts are bone-resorbing cells differentiated from macrophage/monocyte precursors in response to M-CSF and RANKL. *In vitro* models are principally based on primary bone marrow macrophages, but RAW 264.7 cells are frequently used because they are widely available, easy to culture, and more amenable to genetic manipulation than primary cells. Increasing evidence, however, has shown that the vastly different origins of these two cell types may have important effects on cell behavior. In particular, M-CSF is prerequisite for the differentiation of BMMs, by promoting survival and proliferation and priming the cells for RANKL induction. RAW 264.7 cells readily form osteoclasts in the presence of RANKL, but M-CSF is not required. Based on these key differences, we sought to understand their functional implications and how it might affect osteoclast differentiation and related signaling pathways. Using a robust and high-throughput proteomics strategy, we quantified the global protein changes in osteoclasts derived from bone marrow macrophages and RAW 264.7 cells at 1, 3, and 5 days of differentiation. Data are available via ProteomeXchange with identifier PXD009610. Correlation analysis of the proteomes demonstrated low concordance between the two cell types ($R^2 \approx 0.13$). Bioinformatics analysis indicate that RANKL-dependent signaling was intact in RAW 264.7 cells, but biological processes known to be dependent on M-CSF were significantly different; including cell cycle control, cytoskeletal organization, and apoptosis. RAW 264.7 cells exhibited constitutive activation of Erk and Akt that was dependent on the activity of Abelson tyrosine kinase, and the timing of Erk and Akt activation was significantly different between BMMs and RAW 264.7 cells. Our findings provide the first evidence for major differences between BMMs and RAW 264.7 cells, indicating that careful consideration is needed when using the RAW 264.7 cell line when studying M-CSF-dependent signaling and functions.

Keywords: osteoclasts, proteomics, bone marrow macrophages, RAW 264.7, models

INTRODUCTION

Osteoclasts (OCs) are the cells uniquely responsible for resorbing bone, and play important roles in both physiological and pathological bone remodeling.[1-3] In the endeavor to discover new and better treatment strategies against osteoporosis, much effort has been put into elucidating the critical signaling pathways that regulate OC differentiation. In the presence of M-CSF and RANKL, the two cytokines necessary and sufficient for OC differentiation, precursor cells of the hematopoietic lineage undergo a dramatic reconfiguration where they fuse to form expansive, multinucleated OCs. These cells adhere and secrete acids and hydrolases onto the bone surface to resorb bone.[1, 2, 4]

Both bone marrow macrophages (BMMs) and RAW 264.7 cells have the potential to differentiate into OCs, but the vastly different origins of these two cell types may have profound effects on cell signaling and behavior. While BMMs are primary cells most frequently isolated from the marrow cavity of rodent long bones[5], RAW264.7 cells are a transformed macrophage-like cell line derived from the lymphoma of a male BALB/c mouse infected by the Abelson Murine Leukemia Virus (A-muLV).[6, 7] The retrovirus encodes an oncogenic form of the Abelson kinase, v-Abl, which is a fusion protein where portions of the retroviral Gag proteins substitute regions of the SH3 domain of c-Abl, rendering the tyrosine kinase constitutively active.[8-12] Studies have shown that the expression of v-Abl leads to the constitutive activation of mitogenic signaling pathways (e.g. Ras, Jak-Stat, JNK, and PI3K), resulting in uncontrolled cell proliferation—a key feature of cell transformation.[11] In human patients, the fusion protein comprised of the breakpoint cluster region (BCR) and ABL1 (BCR-ABL) causes chronic myeloid leukemia.[13] Patients receiving inhibitors to c-Abl often show reduced bone turnover due to impaired osteoblast (OB) and OC function.[14] These inhibitors can directly suppress OC formation and bone resorption through various mechanisms, including preventing M-CSF-induced phosphorylation of c-Fms.[15, 16] Additionally, BMMs prepared from c-Abl null mice show impaired OC differentiation and reduced TRAP activity.[17] c-Abl undoubtedly plays an important role in OCs, but how the constitutive activity of v-Abl affects the behavior of OCs derived from RAW 264.7 cells is unclear.

The osteoclastogenic potential of RAW264.7 cells was first demonstrated by Hsu *et al.*,[18] who found that RAW 264.7 cells expressed RANK and could readily generate large, $TRAP^+$ cells capable of resorbing bone in the presence of RANKL. RAW 264.7 cells have since been an important cell line for bone research, due to their widespread availability, homogeneous nature of pre-OC population (devoid of osteoblasts, lymphocytes, stroma, etc.), and ease of culture and transfection for genetic manipulation.[19] The significance of RAW 264.7 cells is evidenced by the >530 publications to date that have employed this cell model in OC studies (PubMed). Some among these studies sought to characterize the OCs derived from RAW 264.7 cells and have largely determined that these OCs do indeed mimic their BM-derived counterpart, although some irregularities have raised awareness of fundamental problems that have yet to be rectified.[20, 21] Notably, multiple reports have documented that RAW 264.7 cells can proliferate and undergo OC differentiation independently of M-CSF.[22-25] One study in particular demonstrated that RANKL augments M-CSF production in RAW 264.7 cells, which helps to explain why exogenous M-CSF is not needed.[21] Following these findings, we further investigated the functional differences between RAW 264.7 cells and BMMs in OC differentiation and its related signaling pathways.

Proteomics is a powerful tool that has led to numerous discoveries of proteins and biological processes that drive OC differentiation.[26] Notably, this technique was recently used to map the podosome proteome and helped to advance our understanding of determinants in the macrophage multinucleation process.[27, 28] In other examples, proteomics analysis identified changes in the expression of proteins involved in metabolism and redirection of energy flow towards bone resorption in OCs.[29] Proteomics can therefore provide a broad yet informative overview of the systemic changes in the differentiating OC. We employed a robust and high-throughput liquid-chromatography mass spectrometry (LC-MS)-based proteomics approach to characterize the global protein changes of OCs at different stages of the reprogramming process. Our findings provide the first evidence that BMMs and RAW 264.7 cells are significantly different; especially in processes related to cell

cycle control, cytoskeletal organization, and apoptosis. These results warrant careful consideration when using the RAW 264.7 cell line for studying M-CSF-dependent signaling and functions.

MATERIALS AND METHODS

Materials

The pGEX-4T-1-rRANKL vector was a generous gift from Dr. Steven Teitelbaum that encodes the GST fusion construct containing the biologically active extracellular domain of RANKL (GST-RANKL).[30, 31] The plasmid was transformed into and expressed in a modified *E. Coli* strain Origami B(DE3) cells (EMD Millipore, Billercica, MA, USA) that co-expresses chaperone proteins and was generously provided by Dr. Ding Xu. The GST-RANKL fusion protein was purified using a BioScale Mini Profinity GST cartridge (Bio-Rad, Hercules, CA, USA) and a subsequent size-exclusion chromatography step. Endotoxins were removed using the Pierce High Capacity Endotoxin Removal Resin (Thermo Fisher Scientific, Waltham, MA, USA). GNF-2 was obtained from Selleck Chemicals (Houston, TX, USA).

Isolation of Primary Bone Marrow Cells

Bone marrow cells were obtained from the tibia and femur of 8-week-old C57BL/6J mice as described previously.[32] All studies and procedures performed on mice were approved by the University at Buffalo Institutional Animal Care and Use Committee.

Cell Culture & Osteoclast Differentiation

The RAW 264.7 cell line was obtained from the American Type Culture Collection (ATCC). RAW 264.7 cells and BMMs were cultured in αMEM containing 10% fetal bovine. BMMs and RAW 264.7 cells were treated with M-CSF and RANKL for 0, 1, 3, and 5 days. The method for generating OCs *in vitro* from BMMs was described previously.[5]

Reverse Transcription and Quantitative PCR

Total RNA was isolated from cells using Trizol reagent (Invitrogen) following manufacturer's instructions. cDNA was reverse transcribed from 1 μg total RNA using the RNA to cDNA EcoDry Premix kit (Clontech, Palo Alto, CA, USA). Primer sequences were designed using Primer BLAST [33] and purchased from Integrated DNA Technologies (San Diego, CA, USA). The primer sequences are listed in Supplemental Table 1. All PCR reactions were normalized to the housekeeping gene *Hprt*.[34] qPCR analysis was performed using the 2x SYBR Green qPCR Master Mix (Bimake, Houston, TX, USA) according to manufacturer's instructions. Data analysis of gene expression was performed using the CFX Maestro software (Bio-Rad).

Protein Extraction and Precipitation/ On-Pellet Digestion

Cells were harvested using ice-cold lysis buffer (50 mM Tris-formic acid, 150 mM NaCl, 0.5% sodium deoxycholate, 1% SDS, 2% NP-40, pH 8.0) with protease inhibitor (cOmplete, Mini, EDTA-free; Roche, Mannheim, Germany). Samples were prepared for MS analysis using a previously established method.[35]

Liquid Chromatography-Tandem Mass Spectrometry Analysis

The "IonStar" LC-MS experimental pipeline was developed and optimized in a previous study.[35] Details can be found in the Supplemental Methods. A stringent set of criteria including a low peptide and protein false discovery rate (FDR) of < 1% and ≥2 peptides per protein was used for protein identification. An ion current-based quantification method (IonStar processing pipeline) was described previously.[35] The mass spectrometry proteomics data have been deposited to the ProteomeXchange Consortium via the PRoteomics IDEntifications (PRIDE)[36] partner repository with the dataset identifier PXD009610.

Bioinformatics Analysis

Ingenuity Pathway Analysis (Qiagen, Redwood City, CA, USA) and InnateDB [37] was used to perform gene ontology (GO) term analysis. Hierarchical clustering analysis and heat map visualization were performed using the *heatplot* function in R Package *made4*. Fuzzy C-means clustering was performed using the *cmeans* function in R Package *e1071*, and the results were visualized using the R package *ggplot2* and *viridis* color palette.

Western Blot

Cells were cultured in 6-well plates in complete medium and pretreated with GNF-2 in serum-free medium for 3 hours before induction with either M-CSF (100 ng/mL) or RANKL (200 ng/mL) for the indicated times. BMMs and RAW 264.7 cells were treated with 2 μM and 5 μM GNF-2, respectively. Western blot was performed as described previously.[38] The primary antibodies used in this study were as follows: rabbit polyclonal phosphorylated Akt (Thr308) (1:1000, Cell Signaling Technology), rabbit monoclonal Akt (pan) (1:1000, CST), rabbit polyclonal Erk1 (Thr202/Tyr204) + Erk2 (Thr186/Tyr187) (1:100, Abcam), rabbit polyclonal Erk1/2 (1:1000, CST), and rabbit monoclonal Gapdh (1:2000, CST). Densitomety analysis was performed using ImageJ[39] and normalized to the Gapdh intensity. Relative phosphorylation of Akt and Erk was presented as the ratio between the phosphorylated normalized to the non-phosphorylated/total protein.

Statistical Analysis

The proteomics data are representative of three biological replicates (mice) for BMMs and five replicates for RAW 264.7 cells, for each time-point of OC differentiation (Days 0, 1, 3, and 5). Fold-change values at each time-point were normalized to Day 0 (un-induced) and analyzed by two-tailed Student's *t* test. Proteins demonstrating >0.5 $\log_2$(fold-change) and *p*-values <0.05 were considered statistically significant. Quantitative data are presented as means ± SD from at least three independent experiments and were analyzed using two-tailed Student's *t*-test. A *p*-value of <0.05 was considered statistically significant.

RESULTS

Characterization of the temporal proteome during OC differentiation

Proteomics analysis identified 3,498 and 5,566 quantifiable proteins in the BM- and RAW264.7-derived OCs, respectively, with no missing data at all time-points (1, 3 and 5 days after RANKL induction) (Figure 1A, Supplemental Table 2). 3,148 proteins were shared between both datasets, thereby allowing direct comparison

of the protein expression levels (Figure 1B). Within this shared dataset of proteins, we identified 1,614 unique (non-redundant) proteins that were significantly altered by M-CSF/RANKL in at least one time-point relative to Day 0. Proteins are considered significantly altered if they exceed the thresholds set at *p*-value <0.05 and >0.5 log_2-transformed ratio (Figure 1C). To determine whether the total protein quantities across the time-points were equivalent, we assessed the relative abundance of housekeeping proteins traditionally used as western blotting internal controls (Figure 1D). A previous study by Stephens *et al.*, examined the stability of a set of housekeeping genes, including β-actin (*Actb*), glyceraldehyde 3-phosphate dehydrogenase (*Gapdh*), β2-microglobulin (*B2m*), and hypoxanthine-guanine phosphoribosyltrasnferase (*Hprt*) by qRT-PCR. They determined that *B2m* showed the least variability while *Gapdh* showed the highest variability in BM-derived OCs.[34] When using the same criteria for determining significantly altered proteins in the full dataset, we found that no housekeeping proteins with the exception to B2m and Hprt were significantly altered relative to Day 0. In BMMs, B2m was transiently upregulated while Hprt was downregulated during OC differentiation; none of these proteins, however, were significantly altered in RAW264.7 cells. Because numerous studies have identified major discrepancies in the correlation between mRNA and protein expression levels,[29, 40, 41] we were interested in whether housekeeping proteins exhibited any differences in OCs. In contrast to the findings by Stephens *et al.*, we observed that Gapdh levels were consistent throughout OC differentiation in BMMs, whereas B2m and Hprt were not, indicating that these two proteins may not be reliable internal controls for protein samples. In any case, the stability of common housekeeping proteins such as Actb, Gapdh, α- (Tuba1c), β- (Tubb4a and Tubb4b), and γ-tubulins (Tubg1) in our dataset indicating low intergroup variation reinforces the reliability of the proteomics data.

To validate the biological relevance of our proteomics data, we focused on proteins belonging to the canonical signaling pathways induced by RANKL and M-CSF, including the MAPK, NFκB, PI3K, calcium signaling, and co-stimulatory pathways (Figure 1E and F). OC marker proteins, including Cathepsin K (Ctsk), ATPase H^+ transporting V0 subunit D2 (Atp6v0d2), metalloproteinase 9 (Mmp9), tartrate-resistant acid phosphatase (Trap),

carbonic anhydrase (Cah), and integrin β3 (Itgb3) were dramatically upregulated. The intensities of protein expression were comparable between OCs derived from BMMs and RAW264.7 cells, with the exception of Mmp9, which was more strongly induced in RAW264.7 cells. NFATc1, the master regulator of OC differentiation, was also strongly upregulated, however, BMMs and RAW 264.7 cells demonstrated slightly different kinetics of the protein's expression. In BMMs, NFATc1 upregulation was only significantly starting at Day 3, which was maintained through Day 5 (+1.8 and +1.8, respectively). In RAW264.7 cells, the peak of NFATc1 expression was at Day 1 (+2.2) which gradually decreased at Day 3 and Day 5 (+1.6 and +1.2, respectively). Interestingly, the different patterns of NFATc1 expression did not affect the expression pattern of the OC marker proteins, which were very similar between the two cell types. In addition to NFATc1, RANKL activates other transcription factors important for OC differentiation, including PU.1, c-Fos, NFκB1 (canonical NFκB) and PPARγ, which are known to be activated during the early phase of OC differentiation [(42)]. The proteomics data showed that c-Fos expression was upregulated (+1.0) at Day 1 but not at Days 3 and 5. The other early factors, PU.1 and NFκB1, did not show any upregulation at any of the time-points (Figure 1F). This observation outlines a constraint in our experimental design, such that our data does not cover the early phase response (<24 hours). On the other hand, NFATc1, MITF, and NFκB2 (non-canonical NFκB), which are known to function during the later phase of OC differentiation, were strongly upregulated at the time-points captured in our experiment (Figure 1E and F). Therefore, our proteomics data provide an excellent coverage of signaling pathways important for OC differentiation.

Unsupervised clustering and correlation analysis reveals major differences in the proteomes of BMMs and RAW264.7 cells in the later phases of osteoclastogenesis

To analyze the concordance between the proteome of OCs derived from BMMs or RAW264.7 cells, hierarchical clustering analysis was performed on all proteins shared between both datasets (n = 3,148) (Figure 2A). In general, proteins that were significantly altered at Day 3 maintained the same direction of change (up- or downregulation) into Day 5, but the changes tend to become more pronounced at Day 5. This observation

indicates that the OC progenitors were fully committed by Day 3, and that the same transcriptional program was maintained for the remainder of the differentiation process. When assessing how the proteomes of RAW 264.7 cells and BMMs are related, the predominant clustering pattern was based on cell type, followed by the timing of OC differentiation (Figure 2A). The expression profiles for Day 1 BMMs and RAW264.7 cells showed a moderate degree of similarity, demonstrated by their proximity in the left dendrogram and concordance in the heat map. At Days 3 and 5, however, the expression profiles for BMMs and RAW 264.7 cells significantly diverged. A subset of proteins at Days 3 and 5 exhibited a high degree of concordance (Figure 2A, black bar), but surprisingly, most proteins showed a weak relationship between the two cell types. Overall, our observations suggest that RAW 264.7 cells and BMMs undergo similar processes during early OC differentiation but may have functional differences during the later phases of OC differentiation.

We performed a correlation analysis to mathematically determine the similarity between the expression profiles of BMMs and RAW 264.7 cells during OC differentiation. To establish the experimental "upper-limit" for which the highest correlation could be achieved, we selected twenty OC markers for correlation analysis that included proteins indispensable for OC formation, including nuclear NFATc1, Mmp9, Atp6v0d2, etc. (Figure 2B). Given that both BMMs and RAW264.7 cells readily differentiate into OCs, we expected OC markers to be induced similarly despite any potential differences between these two cell types. As expected, the expression of OC markers was generally proportionate in both cell types, with the exception to Mmp9 and Src. Mmp9 had a more prominent increase in RAW264.7 cells (+5.6) as compared to BM cells (+3.8) at Days 3 and 5. On the other hand, Src in RAW264.7 cells only showed a moderate induction (+1.0) as compared to BM-derived OCs (+2.4). Correlation coefficients (R^2) calculated using the Pearson method showed an increasing correlation strength with time, as evidenced by strong positive values of $R^2 = 0.7637$ and 0.8155 at Days 3 and 5, respectively. When the same analysis was applied to all proteins shared between these two cell types ($n = 3148$), the correlations only demonstrated a weakly positive ($R^2 \approx 0.13$) relationship, indicating significant differences

in the proteomes of OCs differentiated from RAW264.7 or BMM cells, as observed in the hierarchical clustering analysis (Figure 2C).

Cell cycle signaling, cytoskeletal organization, and apoptosis were significantly altered in RAW 264.7 cells compared to BMMs

Given the weak correlation between the proteomes of OCs derived from RAW 264.7 cells and BMMs, we sought to identify the biological processes that were differentially regulated. We first characterized the temporal dynamics of the OC proteome, through examining the significantly altered proteins by fuzzy c-means clustering (Figure. 3A). The analysis revealed eight distinct patterns of protein expression, which were generally similar between RAW 264.7 cells and BMMs. The expression of these proteins was increased in clusters 1, 2, and 3; transiently increased in cluster 4; or decreased in clusters 5, 6, and 8. Although clusters 1, 2, and 3 all contained proteins with increased expression, the different clusters corresponded to different intensities of change. Cluster 1 encompassed proteins that were dramatically increased (2-4 fold-change), while cluster 2 contained proteins with moderate increases (~1 fold-change), and cluster 3 with proteins that were slightly increased (~0.5 fold-change). The same was observed for the downregulated clusters, where cluster 6 (and BMM cluster 7) represented slightly decreased proteins (~0.7 fold-change), cluster 5 for moderately decreased proteins (~1 fold-change), and cluster 8 for intensely decreased proteins (~2 fold-change). In this analysis, we paired the clusters based on their direction and magnitude of change, but we identified a group of proteins in RAW 264.7 cells (cluster 7) whose temporal profile did not have a "mirror" in BMMs. These proteins were transiently decreased at Day 1 but became slightly increased by Days 3 and 5. Furthermore, while clusters 5, 6, and 8 in BMMs demonstrated a steady decline in protein expression at the later time-points, the downregulated proteins in RAW 264.7 were transiently decreased at Days 1 and 3 then slightly increased at Day 5 (Figure 3A). We next performed GO term analysis to determine the biological processes associated with these temporal patterns (Figure 3B). Interestingly, clusters with similar trends and magnitudes of expression were involved in specific biological functions across both cell types. Cluster 1, for example, representing proteins that were strongly

upregulated, was most closely involved in "RANK signaling in osteoclasts". Cluster 2, representing the moderately upregulated proteins, was enriched in "energy metabolism" for both RAW 264.7 cells and BMMs. These observations indicate that the cellular abundance of proteins is tightly regulated during OC differentiation and may be characteristic of particular biological processes. The analysis also revealed several functional differences between the two cell types. First, proteins involved in cell cycle control was significantly overrepresented in BMMs (cluster 7, moderately decreased), but not in RAW 264.7 cells. Correlation analysis of protein expression related to cell cycle control (n = 162) indicated a weak but significant *negative* correlation between RAW 264.7 cells and BMMs at Day 5 (R^2 = 0.0938) (Figure 3C). Closer inspection of these proteins showed that multiple components of the DNA replication complex, notably the members of DNA helicase complex (Mcm2-6), family B DNA polymerases (Polδ1, and ϵ3), ssDNA-stabilizing proteins (Rpa1/3), proliferating cell nuclear antigen (Pcna), and topoisomerases were downregulated to varying degrees in BMMs at Day 3 and Day 5 (Figure 3D, Supplemental Figure 1). In contrast, these proteins were either unchanged or upregulated in RAW264.7 cells. Moreover, cell division protein kinase 6 (Cdk6), an important regulator of G1 phase progression and G1/S transition of the cell cycle, was intensely upregulated at all time-points of OC differentiation in RAW 264.7. In BMMs, Cdk6 was slightly increased at Day 1 but was not significantly changed at Days 3 or 5. Our data indicates that BMMs cease proliferation after the precursor cells have committed to OC differentiation by Day 3. In comparison, RAW 264.7 cells actively proliferate even at the later stages of OC differentiation. This distinction was not unexpected, since uncontrolled proliferation is a hallmark feature of transformed cells such as RAW 264.7 cell line.

OCs derived from BMMs and RAW 264.7 cells are capable of resorbing ivory or hydroxyapatite wafers *in vitro*, but we were interested in whether proteins related to the bone resorption process might be differentially regulated between the two cell types. The GO enrichment analysis revealed a significantly overrepresentation of proteins involved in actin cytoskeleton signaling in RAW 264.7 cells in clusters 6 and 7, respectively (Figure 3B), indicating that these processes were downregulated in RAW 264.7 cells during OC differentiation. In

comparison, the same processes were not as strongly enriched in clusters 5-8 in BMMs. Closer inspection of these proteins revealed numerous inconsistencies in their expression patterns between these two cell types (Figure 3D, Supplemental Figure 2). Correlation analysis of these proteins (n = 66) showed a poor correlation at Days 5 (R^2 = 0.0145)—coefficients that are significantly lower than the global comparisons ($R^2 \approx 0.13$) (Figure 4C). Notably, the proteins (c-Src, α-actinin, paxillin, cofilin-2) that facilitate the formation of podosomes—actin-rich, adhesive structures that form the sealing zone—were upregulated in BMMs during OC differentiation. These proteins, however, were not induced during OC differentiation in RAW 264.7 cells (Figure 3D, Supplemental Figure 2). The data indicate a lower level expression of adhesion related proteins that might influence bone resorption in RAW 264.7 cells.

Because mature OCs are short-lived, we asked whether OCs derived from RAW 264.7 cells, an immortalized cell line, have an extended life span. We therefore focused on this aspect in our analysis, and found that apoptosis signaling was upregulated in BMMs (cluster 3), which was not observed in RAW 264.7 cells (Figure 3B). On the contrary, proteins related to "Myc-mediated apoptosis" was downregulated in RAW 264.7 cells (cluster 6). Correlation analysis of these proteins revealed no correlation in the expression levels between RAW 264.7 cells and BMMs at Day 5 (R^2 = 0.0056, p = 0.5500) (Figure 3C). In BMMs, the pro-apoptotic factors, BH3 interacting-domain death agonist (Bid), caspase recruitment domain-containing protein 9 (Card9), and caspase-6 and -8 (Casp6/8) were slightly upregulated at Day 3 and sustained into Day 5 (Figure 3D), suggesting that apoptosis signaling was initiated as early as Day 3 of OC differentiation in BMMs. In contrast, the pro-apoptotic regulators such as apoptosis protease activating factor 1 (Apaf1), Card9, and caspase-7 (Casp7) were downregulated in RAW 264.7 cells during later phase OC differentiation. As such, our proteomics data suggest that apoptosis signaling is altered in OCs derived from the immortalized RAW 264.7 cell line compared to BMMs.

Osteoclasts derived from RAW 264.7 cells have extended lifespans as compared to BMMs

To further confirm the above finding regarding apoptosis, we compared the lifespans of OCs differentiated from RAW 264.7 cells and BMMs *in vitro* (Figure 4A and B). At the peak of OC differentiation (Day 5), approximately 9.2 ± 3.8% of OCs have undergone apoptosis in both RAW 264.7 cells and BMMs. When the OCs were maintained for an additional 16 hours, 77.8 ± 11.4% OCs have undergone apoptosis in BMMs, as compared to the 42.2 ± 9.5% in RAW 264.7 cells. When the OCs were swapped into media without M-CSF/RANKL and cultured for an additional 16 hours, almost all OCs from BMMs have undergone apoptosis (98.9 ± 2.3%) but 78.0 ± 3.0% of OCs differentiated from RAW 264.7 showed apoptotic morphology (Figure 4C and D). In either condition where M-CSF/RANKL were maintained or removed, significantly more OCs derived from RAW 264.7 cells remained after 16 hours. Similar results were obtained when assessing the number of $TUNEL^+$ nuclei in cells depleted of M-CSF/RANKL (Figure 4E). This finding demonstrates that OCs from RAW 264.7 cells have an extended lifespan or are more resilient to apoptosis as compared to OCs derived from BMMs.

Abl is expressed in BMMs and RAW 264.7 cells and is required for osteoclastogenesis

We next sought to reconcile the observed functional differences with the fundamental property of RAW 264.7 cells—a cell line immortalized by the transforming activity of v-Abl. Although the transforming activity of v-Abl has been well characterized, it is not known how this constitutively activated tyrosine kinase affects OC differentiation and function. A previous study showed that GNF-2, a selective inhibitor of Abl kinase activity, dose-dependently inhibited the proliferation of OC precursors through the suppression of c-Fms-dependent signaling. GNF-2 also accelerated OC apoptosis by inducing caspase-3 and Bcl-2-like protein 11 (Bim) expression, interfered with actin cytoskeletal organization, and blocked the bone-resorbing activity of mature OCs.[43] Based on the consistency of our proteomics data to these findings, we predicted that altered Abl activity was likely responsible for the functional differences observed in RAW 264.7 cells. To test this hypothesis, we investigated whether the signaling downstream of Abl was regulated differently between these two cell types.

RT-PCR analysis using primers annealing to multiple regions of the a-MuLV transcript confirmed that the viral transgene, v-Abl, was specifically expressed in RAW 264.7 cells and not present in primary BMMs (Figure 5A and B). We also performed qPCR analysis to determine the relative expression of v- and c-Abl. Primers that span the Gag and Abl domains are specific for v-Abl. As was demonstrated by the RT-PCR analysis, v-Abl was only expressed in RAW 264.7 cells (Figure 5C). c-Abl on the other hand was expressed in both cell types and was significantly upregulated by M-CSF and RANKL. (Figure 5C). In agreement with previous findings, GNF-2 was a potent inhibitor of OC differentiation in both RAW 264.7 cells and BMMs, demonstrating that Abl is required for osteoclastogenesis (Figure 5D and E).

Constitutive activation of Akt and Erk in RAW 264.7 cells are dependent on Abl

Since Abl was previously shown to regulate c-Fms phosphorylation, we investigated whether M-CSF-dependent activation of Akt and Erk1/2 was altered in RAW 264.7 cells. BMMs and RAW 264.7 cells were serum-starved and pretreated with GNF-2 for 2 hours then induced with M-CSF for the indicated times (Figure 6A and B). Consistent with previous reports, M-CSF treatment induced a potent and transient activation of Akt and Erk1/2 in BMMs (Figure 6A and B).[44] In RAW 264.7 cells, Erk1/2 was phosphorylated even in the absence of M-CSF, and the basal activation was sustained throughout the duration of experiment. GNF-2 inhibited the basal and induced phosphorylation of Erk1/2 (Figure 6A and B), suggesting that v-Abl was responsible for the constitutive activation of Akt and Erk1/2 in RAW 264.7 cells. Interestingly, GNF-2 treatment reduced the total abundance of Akt in BMMs but not in RAW 264.7 cells. Given that M-CSF-dependent signaling was regulated differently between RAW 264.7 cells and BMMs, we next determined how these cells respond to RANKL (Figure 6C and D). As before, the basal p-Akt level in RAW 264.7 cells was relatively higher than that observed in BMMs. In response to RANKL, BMMs showed a gradual increase in Akt phosphorylation over time whereas in RAW 264.7 cells, it was transiently decreased and reverted to original levels by 2 hours of induction (Figure 6C and D). Additionally, p-Erk1/2 was sharply induced at 15 minutes of RANKL treatment but reverted to basal levels at 30 minutes and onwards in BMMs. In contract, RAW 264.7

cells demonstrated a gradual induction of p-Erk1/2 that reached its maximum at 30 minutes of RANKL treatment that slowly declined afterwards; and the rate of p-Erk1/2 induction coincided with the decline of p-Akt. Overall, the data indicated that the M-CSF- and RANKL-dependent phosphorylation of Akt and Erk1/2, effector molecules downstream of Abl, were differentially regulated between BMMs and RAW 264.7 cells (Figure 6E).

DISCUSSION

The RAW 264.7 cell line has undoubtedly been an important research tool in the study of OCs, in part because they are easy to handle and manipulated, unlike BMMs, which can often be inconsistent in differentiation efficiency. Despite the extensive use of RAW 264.7 cells in our community over the past 18 years, surprisingly few studies have sought to characterize and compare them to the primary BMMs, to which they are supposed to model. This concern is especially disconcerting given that fundamental differences clearly exist, but no clear mechanism delineates the two cell models, and therefore it is not known whether OCs derived from RAW 264.7 cells can wholly replicate the behavior of the primary BMMs.

We employed a cutting-edge proteomics strategy that pushes the boundaries of protein identification and quantification[35]; consequently, our study provides the most comprehensive coverage of the OC proteome to date. In two most recent proteomics studies of OC differentiation from RAW 264.7 cells, one study identified 2,068 non-redundant proteins (defined as ≥2 peptides per protein for identification with a 5% FDR)[29] and the other identified 3,729 unique proteins (≥2 peptides/protein and 1% FDR).[45] In comparison, our study reliably identified 5,566 unique proteins, a 49.2% increase in coverage, in RAW 264.7 cells using a similarly stringent criteria of ≥2 peptides per protein for identification with a 5% FDR (Figure 1A). Moreover, the majority of OC proteome studies have been confined to RAW 264.7 cells.[26] To the best of our knowledge, our study is the first to investigate the proteome of OCs differentiated from BMMs [26, 46], which is often regarded to be more faithful to the mouse *in vivo* system as compared to RAW 264.7 cells. Our proteomics analysis identified a total of

3,498 unique proteins for BMMs. The lower number of proteins identified may be attributed to the heterogeneous nature of total bone marrow, which could result in fewer proteins that meet the peptides per protein identification criterion. Nonetheless, the proteomics data produced in this study will prove to be useful by updating the current OC proteome database with a substantially more comprehensive dataset. Furthermore, the BMM-based OC dataset represents a rich trove of information for future data-mining endeavors.

More importantly, this study outlines the first targeted and in-depth analysis of differences between two prominent OC cell models from a molecular standpoint. A previous study compared the gene expression profiles of OCs derived from RAW 264.7 cells to that of primary cells, and found that amongst the 405 genes used for the analysis, the two cell types expressed largely the same complement of genes (R^2 = 0.7599).[20] In comparison, our correlation analysis determined a substantially lower correlation coefficient of R^2 = 0.1365 (Day 5) (Figure 2C). Several plausible reasons might account this large discrepancy. First, the previous study used clonal populations of RAW 264.7 cells deemed to possess high osteoclastogenic potential; using purified precursor cells could enrich for genes related to OC differentiation. Second, numerous studies have consistently shown that gene expression levels do not correlate well with protein abundance; this phenomenon could therefore contribute to the discrepancy between the correlation analyses based on cDNA levels versus protein levels.[29, 40, 41] In line with this thought, we assessed the protein levels of housekeeping genes reported to be stable at the transcript level in OCs, and found that transcript and protein levels for some of these genes to be inconsistent (Figure 1D).[34] Third, the correlation analysis in the previous study observed only the proteins strongly induced during OC differentiation, potentially imparting selection bias to the results, whereas our analysis included the entire set of proteins identified. This phenomenon can be observed in the fuzzy c-means clustering analysis, which showed that the most strongly upregulated proteins were strongly correlated between RAW 264.7 cells and BMMs, as these proteins were frequently involved in fundamental aspects of OC differentiation (Figures 3A and B). Similarly, when we performed the correlation analysis on proteins involved in the canonical signaling pathways of OC differentiation, which incidentally had the highest expression levels,

the correlation coefficient reached as high as $R^2 = 0.8155$, bringing the score closer to that in the previous study (Figure 2B). Therefore, correlation analyses performed on a filtered subset of proteins could inadvertently produce skewed results, which is why we chose to perform the analysis on an unfiltered dataset. Overall, our correlation analysis indicates that substantial inconsistencies exist within the proteomes of OCs derived from RAW 264.7 cells and BMMs.

Our comparative study unveiled a diverse set of biological processes that were differentially regulated between RAW 264.7 cells and BMMs during OC differentiation. Specifically, the regulation of proteins involved in cell cycle control, cytoskeleton reorganization, and apoptosis were significantly dissimilar. The coordinated actions of cell cycle withdrawal, initiation of differentiation-associated gene expression, and cellular reorganization are key steps in the terminal differentiation of cells [47]. In fact, studies have shown that OC progenitors withdraw from the cell cycle and are post-mitotic at the time of fusion and terminal differentiation.[48, 49] Consistent with previous findings, our results show that BMMs downregulated proteins involved with cell cycle control and chromosomal replication at Days 3 and 5 of differentiation; RAW 264.7 cells, however, exhibited an opposite trend (Figure 3C). Notably, Cdk6 and Pcna were among the most highly upregulated proteins related to cell cycle control in RAW 264.7 cells. This observation does not, however, necessarily indicate that OCs from RAW 264.7 cells are actively proliferating at the terminal stages of differentiation. A previous study demonstrated that RANKL could dose-dependently suppress proliferation in RAW 264.7 cells, likely due to cell cycle arrest caused by the downregulation of cyclin D1, D3, and E.[50] Consistent with previous findings, our proteomics analysis found that cyclin D1 to be strongly downregulated in RAW 264.7 cells during the course of OC differentiation (Figure 3D, Supplemental Figure 1).

It has been reported that Abl plays prominent roles in regulating cytoskeletal rearrangement. Abl can coordinate changes to the cytoskeletal structure by regulating the activity of Rho family GTPases, stimulating the assembly of protein complexes that facilitate actin nucleation, or directly interacting with F-actin and microtubules.[51]

Moreover, the constitutive activation of Abl was shown to reduce paxillin phosphorylation and in turn reduce cell adhesion in murine fibroblasts.[52] Interestingly, our result showed that a set of proteins involved in cell adhesion were upregulated in BMMs but not RAW 264.7 cells (Figure 3D, Supplemental Figure 2). Additionally, paxillin expression was slightly downregulated in RAW 264.7 cells and upregulated in BMMs (Figure 3D). Therefore, our proteomics data indicate that RAW 264.7 cells have reduced expression of proteins involved in focal adhesion assembly and sealing zone formation.

Previous work has demonstrated a role for Abl in OC formation by regulating the phosphorylation of c-Fms and the downstream effector molecules Erk and Akt.[53-55] Conversely, GNF-2, an inhibitor of Abl, suppressed M-CSF-dependent activation of Erk and Akt, inhibited the proliferation and differentiation of OCs, interfered with actin cytoskeletal organization, and accelerated apoptosis of mature OCs.[43] Consistent with these reports, we found the aforementioned biological processes to be significantly altered in RAW 264.7 cells as compared to BMMs (Figure 5A). Building on this hypothesis, we found that Abl-related signaling through Erk and Akt showed a low yet constitutive activation in RAW 264.7 cells, and the temporal patterns of activation in response to M-CSF and RANKL were distinct between these two cell types (Figure 6A and B). Despite the differences in Erk and Akt signaling in RAW 264.7 cells, our analysis demonstrated an exceptionally positive and linear correlation in the expression of RANKL-dependent proteins (Figure 2C), indicating that RANKL-dependent signaling was intact in RAW 264.7 cells. A recent study demonstrated that M-CSF induced an immediate effect (5 to 20 min) on Erk phosphorylation whereas RANKL triggered a biphasic activation—an immediate activation (5 to 20 min) and a delayed activation (8 to 24 hours). The second wave of Erk activation coincided with the onset of OC differentiation, indicated by the presence of $TRAP^+$ mononuclear cells and the expression of marker proteins.[56] Because we did not assess this aspect in our study, it is possible that the delayed activation was unaffected in RAW 264.7 cells, and therefore the cell line can still form OCs normally. The evidence from our study collectively indicate that the effects of v-Abl in RAW 264.7 cells were limited to M-

CSF-related signaling pathways. Therefore, our data suggest cautious consideration when using RAW 264.7 cells in future studies investigating signaling and processes downstream of M-CSF.

Irregularities in RAW 264.7 cells such as its independence from M-CSF is a well-known phenomenon, but its effects on the practicality of the cell line as a model remained an important gap in knowledge. Our study indicates that the physiological effects of the transformed state on RAW 264.7 cells may be more significant than previously anticipated. Functions related to cell cycle control, cytoskeletal reorganization, and apoptosis signaling are likely affected in RAW 264.7 cells. Given the involvement of v-Abl, other processes downstream of M-CSF may also be implicated. In light of this, our proteomics data can be a valuable resource to other investigators to avoid potential pitfalls associated with RAW 264.7 cells.

ACKNOWLEDGMENTS

This work was supported by the National Institute of Arthritis and Musculoskeletal and Skin Diseases (NIAMS, AR061052), the National Institute of Aging (NIA, AG048388) awarded to Dr. Shuying Yang, and the Mark Diamond Research Fund (MDRF, SU-17-13) awarded to Andrew Ng.

Authors' roles: AN, CT and SS performed proteomic analysis and data analysis. AN performed cell and molecular biology studies. AN, SY, and JQ completed the manuscript writing and revision. SY, JQ, DX and MJO conceived the study, assisted the data analysis, and edited manuscript.

REFERENCES

1. Boyle WJ, Simonet WS, Lacey DL. Osteoclast differentiation and activation. Nature. 2003;423(6937):337-42.
2. Teitelbaum SL, Ross FP. Genetic regulation of osteoclast development and function. Nat Rev Genet. 2003;4(8):638-49.
3. Martin TJ. Bone biology and anabolic therapies for bone: current status and future prospects. J Bone Metab. 2014;21(1):8-20.
4. Teitelbaum SL. Osteoclasts: What do they do and how do they do it? Am J Pathol. 2007;170(2):427-35.
5. Takahashi N, Udagawa N, Kobayashi Y, Suda T. Generation of osteoclasts in vitro, and assay of osteoclast activity. Methods Mol Med. 2007;135:285-301.
6. Abelson HT, Rabstein LS. Lymphosarcoma: virus-induced thymic-independent disease in mice. Cancer Res. 1970;30(8):2213-22.
7. Raschke WC, Baird S, Ralph P, Nakoinz I. Functional macrophage cell lines transformed by Abelson leukemia virus. Cell. 1978;15(1):261-7.
8. Goff SP, Gilboa E, Witte ON, Baltimore D. Structure of the Abelson Murine Leukemia-Virus Genome and the Homologous Cellular Gene - Studies with Cloned Viral-DNA. Cell. 1980;22(3):777-85.
9. Srinivasan A, Reddy EP, Aaronson SA. Abelson Murine Leukemia-Virus - Molecular-Cloning of Infectious Integrated Proviral DNA. P Natl Acad Sci-Biol. 1981;78(4):2077-81.
10. Reddy EP, Smith MJ, Srinivasan A. Nucleotide-Sequence of Abelson Murine Leukemia-Virus Genome - Structural Similarity of Its Transforming Gene-Product to Other Onc Gene-Products with Tyrosine-Specific Kinase-Activity. P Natl Acad Sci-Biol. 1983;80(12):3623-7.
11. Shore SK, Tantravahi RV, Reddy EP. Transforming pathways activated by the v-Abl tyrosine kinase. Oncogene. 2002;21(56):8568-76.
12. Rosenberg N, Witte ON. The viral and cellular forms of the Abelson (abl) oncogene. Adv Virus Res. 1988;35:39-81.
13. Ren R. Mechanisms of BCR-ABL in the pathogenesis of chronic myelogenous leukaemia. Nat Rev Cancer. 2005;5(3):172-83.
14. Atallah E, Kantarjian H, Cortes J. Emerging safety issues with imatinib and other Abl tyrosine kinase inhibitors. Clin Lymphoma Myeloma. 2007;7 Suppl 3:S105-12.
15. Dewar AL, Cambareri AC, Zannettino AC, et al. Macrophage colony-stimulating factor receptor c-fms is a novel target of imatinib. Blood. 2005;105(8):3127-32.
16. El Hajj Dib I, Gallet M, Mentaverri R, Sevenet N, Brazier M, Kamel S. Imatinib mesylate (Gleevec) enhances mature osteoclast apoptosis and suppresses osteoclast bone resorbing activity. Eur J Pharmacol. 2006;551(1-3):27-33.
17. Ghosh-Choudhury N, Mandal CC, Das F, Ganapathy S, Ahuja S, Ghosh Choudhury G. c-Abl-dependent molecular circuitry involving Smad5 and phosphatidylinositol 3-kinase regulates bone morphogenetic protein-2-induced osteogenesis. J Biol Chem. 2013;288(34):24503-17.
18. Hsu HL, Lacey DL, Dunstan CR, et al. Tumor necrosis factor receptor family member RANK mediates osteoclast differentiation and activation induced by osteoprotegerin ligand. P Natl Acad Sci USA. 1999;96(7):3540-5.
19. Collin-Osdoby P, Osdoby P. RANKL-Mediated Osteoclast Formation from Murine RAW 264.7 cells. Methods Mol Biol. 2012;816:187-202.
20. Cuetara BL, Crotti TN, O'Donoghue AJ, McHugh KP. Cloning and characterization of osteoclast precursors from the RAW264.7 cell line. In Vitro Cell Dev Biol Anim. 2006;42(7):182-8.
21. Islam S, Hassan F, Tumurkhuu G, et al. Receptor activator of nuclear factor-kappa B ligand induces osteoclast formation in RAW 264.7 macrophage cells via augmented production of macrophage-colony-stimulating factor. Microbiol Immunol. 2008;52(12):585-90.
22. Srivastava S, Toraldo G, Weitzmann MN, Cenci S, Ross FP, Pacifici R. Estrogen decreases osteoclast formation by down-regulating receptor activator of NF-kappa B ligand (RANKL)-induced JNK activation. Journal of Biological Chemistry. 2001;276(12):8836-40.
23. Wei S, Teitelbaum SL, Wang MWH, Ross FP. Receptor activator of nuclear factor-kappa B ligand activates nuclear factor-kappa B in osteoclast precursors. Endocrinology. 2001;142(3):1290-5.
24. Sugatani T, Alvarez U, Hruska KA. PTEN regulates RANKL- and osteopontin-stimulated signal transduction during osteoclast differentiation and cell motility. Journal of Biological Chemistry. 2003;278(7):5001-8.

25. Toyomura T, Murata Y, Yamamoto A, et al. From lysosomes to the plasma membrane - Localization of vacuolar type H+-ATPase with the a3 isoform during osteoclast differentiation. Journal of Biological Chemistry. 2003;278(24):22023-30.
26. Segeletz S, Hoflack B. Proteomic approaches to study osteoclast biology. Proteomics. 2016;16(19):2545-56.
27. Rotival M, Ko JH, Srivastava PK, et al. Integrating phosphoproteome and transcriptome reveals new determinants of macrophage multinucleation. Mol Cell Proteomics. 2015;14(3):484-98.
28. Cervero P, Himmel M, Kruger M, Linder S. Proteomic analysis of podosome fractions from macrophages reveals similarities to spreading initiation centres. Eur J Cell Biol. 2012;91(11-12):908-22.
29. An E, Narayanan M, Manes NP, Nita-Lazar A. Characterization of functional reprogramming during osteoclast development using quantitative proteomics and mRNA profiling. Mol Cell Proteomics. 2014;13(10):2687-704.
30. Lam J, Nelson CA, Ross FP, Teitelbaum SL, Fremont DH. Crystal structure of the TRANCE/RANKL cytokine reveals determinants of receptor-ligand specificity. J Clin Invest. 2001;108(7):971-9.
31. Nelson CA, Warren JT, Wang MW, Teitelbaum SL, Fremont DH. RANKL employs distinct binding modes to engage RANK and the osteoprotegerin decoy receptor. Structure. 2012;20(11):1971-82.
32. Yang S, Li YP. RGS12 is essential for RANKL-evoked signaling for terminal differentiation of osteoclasts in vitro. J Bone Miner Res. 2007;22(1):45-54.
33. Ye J, Coulouris G, Zaretskaya I, Cutcutache I, Rozen S, Madden TL. Primer-BLAST: a tool to design target-specific primers for polymerase chain reaction. BMC Bioinformatics. 2012;13:134.
34. Stephens AS, Stephens SR, Morrison NA. Internal control genes for quantitative RT-PCR expression analysis in mouse osteoblasts, osteoclasts and macrophages. BMC Res Notes. 2011;4:410.
35. Shen X, Shen S, Li J, et al. An IonStar Experimental Strategy for MS1 Ion Current-Based Quantification Using Ultrahigh-Field Orbitrap: Reproducible, In-Depth, and Accurate Protein Measurement in Large Cohorts. J Proteome Res. 2017;16(7):2445-56.
36. Vizcaino JA, Csordas A, Del-Toro N, et al. 2016 update of the PRIDE database and its related tools. Nucleic Acids Res. 2016;44(22):11033.
37. Breuer K, Foroushani AK, Laird MR, et al. InnateDB: systems biology of innate immunity and beyond--recent updates and continuing curation. Nucleic Acids Res. 2013;41(Database issue):D1228-33.
38. Yuan X, Cao J, He X, et al. Ciliary IFT80 balances canonical versus non-canonical hedgehog signalling for osteoblast differentiation. Nat Commun. 2016;7:11024.
39. Schindelin J, Arganda-Carreras I, Frise E, et al. Fiji: an open-source platform for biological-image analysis. Nat Methods. 2012;9(7):676-82.
40. Wilhelm M, Schlegl J, Hahne H, et al. Mass-spectrometry-based draft of the human proteome. Nature. 2014;509(7502):582-7.
41. Vogel C, Marcotte EM. Insights into the regulation of protein abundance from proteomic and transcriptomic analyses. Nat Rev Genet. 2012;13(4):227-32.
42. Grigoriadis AE, Wang ZQ, Cecchini MG, et al. c-Fos: a key regulator of osteoclast-macrophage lineage determination and bone remodeling. Science. 1994;266(5184):443-8.
43. Kim HJ, Yoon HJ, Choi JY, Lee IK, Kim SY. The tyrosine kinase inhibitor GNF-2 suppresses osteoclast formation and activity. J Leukocyte Biol. 2014;95(2):337-45.
44. Bradley EW, Ruan MM, Vrable A, Oursler MJ. Pathway crosstalk between Ras/Raf and PI3K in promotion of M-CSF-induced MEK/ERK-mediated osteoclast survival. J Cell Biochem. 2008;104(4):1439-51.
45. Itou T, Maldonado N, Yamada I, et al. Cystathionine gamma-lyase accelerates osteoclast differentiation: identification of a novel regulator of osteoclastogenesis by proteomic analysis. Arterioscler Thromb Vasc Biol. 2014;34(3):626-34.
46. Zhang H, Recker R, Lee WN, Xiao GG. Proteomics in bone research. Expert Rev Proteomics. 2010;7(1):103-11.
47. Ruijtenberg S, van den Heuvel S. Coordinating cell proliferation and differentiation: Antagonism between cell cycle regulators and cell type-specific gene expression. Cell Cycle. 2016;15(2):196-212.
48. Tanaka S, Takahashi N, Udagawa N, et al. Macrophage colony-stimulating factor is indispensable for both proliferation and differentiation of osteoclast progenitors. J Clin Invest. 1993;91(1):257-63.
49. Sankar U, Patel K, Rosol TJ, Ostrowski MC. RANKL coordinates cell cycle withdrawal and differentiation in osteoclasts through the cyclin-dependent kinase inhibitors p27KIP1 and p21CIP1. J Bone Miner Res. 2004;19(8):1339-48.

50. Bharti AC, Takada Y, Shishodia S, Aggarwal BB. Evidence that receptor activator of nuclear factor (NF)-kappaB ligand can suppress cell proliferation and induce apoptosis through activation of a NF-kappaB-independent and TRAF6-dependent mechanism. J Biol Chem. 2004;279(7):6065-76.
51. Koleske AJ. Regulation of Cytoskeletal Dynamics and Cell Morphogenesis by Abl Family Kinases. Austin, TX: Landes Bioscience; 2003-2013.
52. Cheng K, Kurzrock R, Qiu X, et al. Reduced focal adhesion kinase and paxillin phosphorylation in BCR-ABL-transfected cells. Cancer. 2002;95(2):440-50.
53. Dewar AL, Cambareri AC, Zannettino ACW, et al. Macrophage colony-stimulating factor receptor c-fms is a novel target of imatinib. Blood. 2005;105(8):3127-32.
54. Brownlow N, Mol C, Hayford C, Ghaem-Maghami S, Dibb NJ. Dasatinib is a potent inhibitor of tumour-associated macrophages, osteoclasts and the FMS receptor. Leukemia. 2009;23(3):590-4.
55. Vandyke K, Dewar AL, Diamond P, et al. The Tyrosine Kinase Inhibitor Dasatinib Dysregulates Bone Remodeling Through Inhibition of Osteoclasts In Vivo. Journal of Bone and Mineral Research. 2010;25(8):1759-70.
56. Lee K, Chung YH, Ahn H, Kim H, Rho J, Jeong D. Selective Regulation of MAPK Signaling Mediates RANKL-dependent Osteoclast Differentiation. Int J Biol Sci. 2016;12(2):235-45.

FIGURE LEGENDS

Figure 1. High-throughput proteomics analysis accurately maps the global protein changes during OC differentiation. (A) Proteomics experimental design. The proteomics data are representative of $n = 3$ biological replicates (mice) for BMMs and $n = 5$ replicates for RAW 264.7 cells. (B) Venn diagram summarizing the proteins that overlap between the RAW264.7 and BMM datasets. (C) Protein expression changes in RAW 264.7 cells and BMMs during osteoclast development relative to Day 0. Cutoffs using p-value < 0.05 and $\log_2$-transformed ratio of > 0.5 were applied to determine significantly altered proteins. Numbers in the corners of each quadrant indicate the number of proteins that were upregulated (red) or downregulated (green). (D) Relative quantification of common internal control proteins at different time-points of OC differentiation to demonstrate equivalence of protein amounts in each group. (E) The expression of OC marker proteins relative to Day 0. (F) Summary of canonical pathways activated during OC differentiation. Data are means ± SD. Statistical analysis was performed using Student's *t*-test for each time-point against Day 0 (*$p < 0.05$). *GO, gene ontology*.

Figure 2. Unsupervised hierarchical clustering and correlation analysis reveals major differences in the proteomes of BMMs and RAW264.7 cells. (A) Protein expression changes in BMMs and RAW264.7 cells differentiated using M-CSF and RANKL for 1, 3, or 5 days. Heat map of all identified proteins ($n = 3{,}148$) analyzed by hierarchical clustering analysis. (B) Pearson correlation analysis of OC differentiation marker protein expression ($n = 20$) in RAW264.7- and BMM-derived osteoclasts show a strong positive correlation between the two cell models. (C) The same analysis applied to the entire dataset ($n = 3{,}148$), however, revealed a relatively poor correlation ($R^2 \approx 1.3$). Expression values are $\log_2$-transformed ratios relative to Day 0.

Figure 3. Comparative analysis of temporal expression profiles identified diverse biological processes significantly different between RAW 264.7 cells and BMMs. (A) Fuzzy c-means clustering of significantly altered proteins to determine the temporal patterns that characterize the OC proteome. Membership scores indicate the degree to which proteins belong in each cluster. The number of proteins belonging to each cluster is indicated in the table below. (B) Gene ontology term analysis for biological processes that represents the proteins in each fuzzy c-means cluster. Red bolded terms indicate biological processes that were strongly enriched and/or strongly contrasted between RAW 264.7 cells and BMMs. (C) Pearson correlation analysis applied to proteins involved in cell cycle signaling, cytoskeletal organization, and apoptosis signaling at Day 5 of OC differentiation. (D) Table of key proteins found to be poorly or negatively correlated between RAW 264.7 cells and BMMs.

Figure 4. Osteoclasts derived from RAW 264.7 cells have extended lifespans as compared to BMMs. (A) TRAP staining of OCs derived from RAW 264.7 cells and BMMs induced with M-CSF and RANKL for 2-6 days. (B) The number of dead OCs were quantified and presented as a percentage of the total number of OCs. (C, D) TRAP staining of mature OCs depleted of M-CSF and RANKL for 16 hours. (E). Percentage of $TUNEL^{+}$ nuclei in mature OCs depleted of M-CSF and RANKL for 16 hours. Scale bar = 1 mm. Data are means ± SD. Statistical analysis was performed using Student's *t*-test (*$p < 0.05$, ***$p < 0.001$).

Figure 5. The viral oncogene v-Abl is expressed in RAW 264.7 cells and Abl is required for osteoclastogenesis. (A) Diagram illustrating the structure of the integrated Abelson murine leukemia virus (a-MuLV) genome and the relative regions amplified by RT-PCR (black bars). LTR, long terminal repeats; MMLVΨ, Moloney murine leukemia virus Psi packaging element; Gag, group-specific antigen; Abl, Abelson tyrosine kinase. (B) RT-PCR was used to detect the various components of the a-MuLV genome in RAW 264.7 and BMMs treated with or without M-CSF/RANKL for 48 hours. (C) The relative expression of v- and c-Abl were determined by qPCR and signals were normalized to *Hprt*. (D) TRAP staining of OCs treated with DMSO

(vehicle) or the Abl inhibitor GNF-2 (2 μM). (E) The number of $TRAP^+$, multinucleated (>10 nuclei) cells were counted. Scale bar = 1 mm. Data are means ± SD. Statistical analysis was performed using Student's *t*-test (**p* < 0.05, ***p* <0.01, ****p* < 0.001).

Figure 6. Constitutive activation of Akt and Erk1/2 in RAW 264.7 cells are dependent on Abl. (A, B) M-CSF-dependent phosphorylation of Akt and Erk1/2 in OC progenitor cells starved and pre-treated with DMSO (vehicle) or GNF-2 in serum-free medium for 2 hours. Cells were treated with 100 ng/mL M-CSF for the indicated times and analyzed by western blotting. (C, D) Time-course of RANKL-dependent phosphorylation of Akt and Erk1/2 in BMMs and RAW 264.7 cells serum-starved and pre-treated with DMSO or GNF-2 for 2 hours and stimulated using 200 ng/mL RANKL for the indicated times. (E) Model of Abl-dependent signaling pathway in OCs. Densitomety analysis was performed using ImageJ and normalized to the Gapdh intensity. Relative phosphorylation of Akt and Erk was presented as the ratio between the phosphorylated normalized to the non-phosphorylated/total protein. Data are means ± SD. Statistical analysis was performed using Student's *t*-test (**p* < 0.05, ***p* < 0.01 ****p* < 0.001).

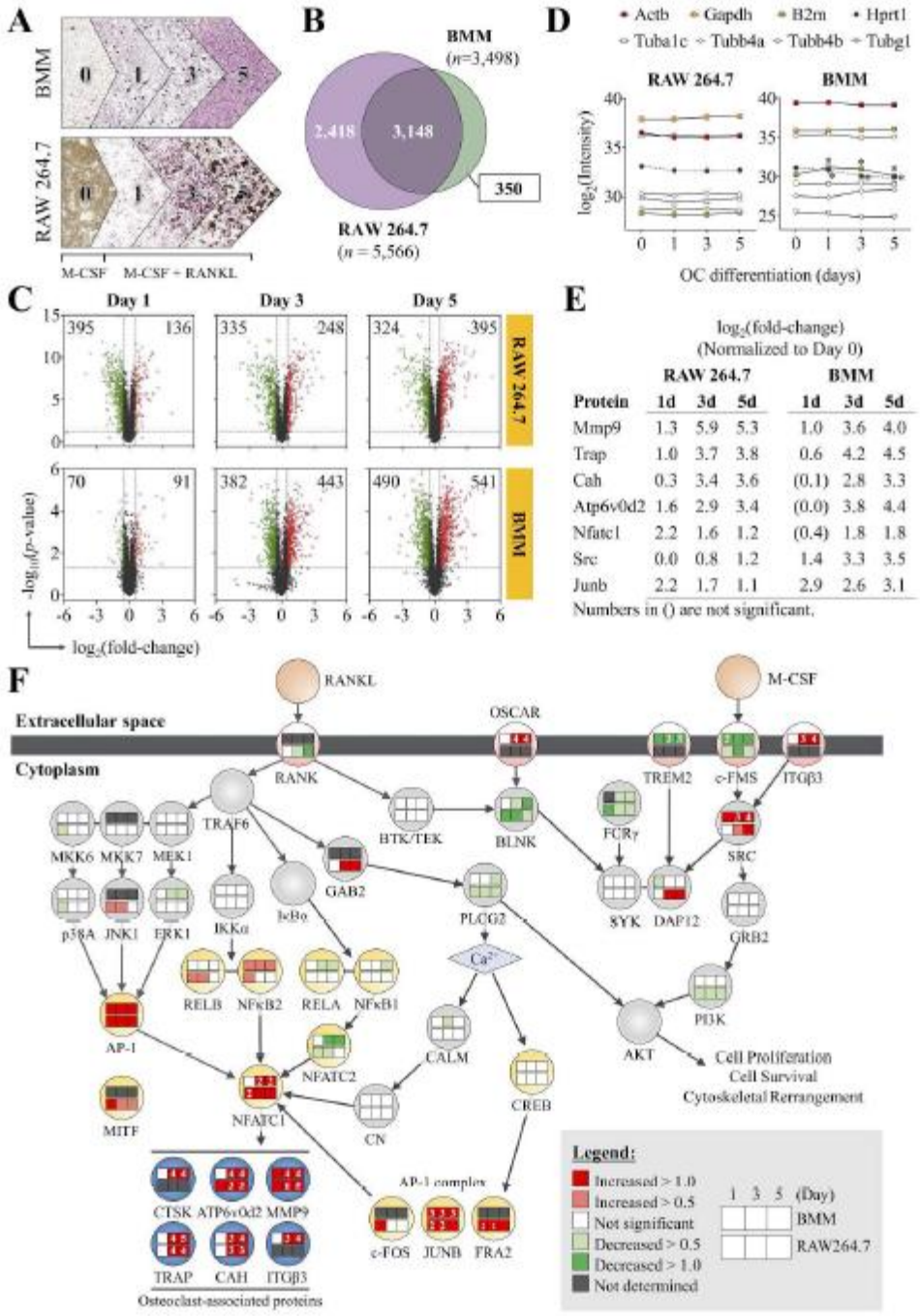

Protein	RAW 264.7 1d	RAW 264.7 3d	RAW 264.7 5d	BMM 1d	BMM 3d	BMM 5d
Mmp9	1.3	5.9	5.3	1.0	3.6	4.0
Trap	1.0	3.7	3.8	0.6	4.2	4.5
Cah	0.3	3.4	3.6	(0.1)	2.8	3.3
Atp6v0d2	1.6	2.9	3.4	(0.0)	3.8	4.4
Nfatc1	2.2	1.6	1.2	(0.4)	1.8	1.8
Src	0.0	0.8	1.2	1.4	3.3	3.5
Junb	2.2	1.7	1.1	2.9	2.6	3.1

Figure 1

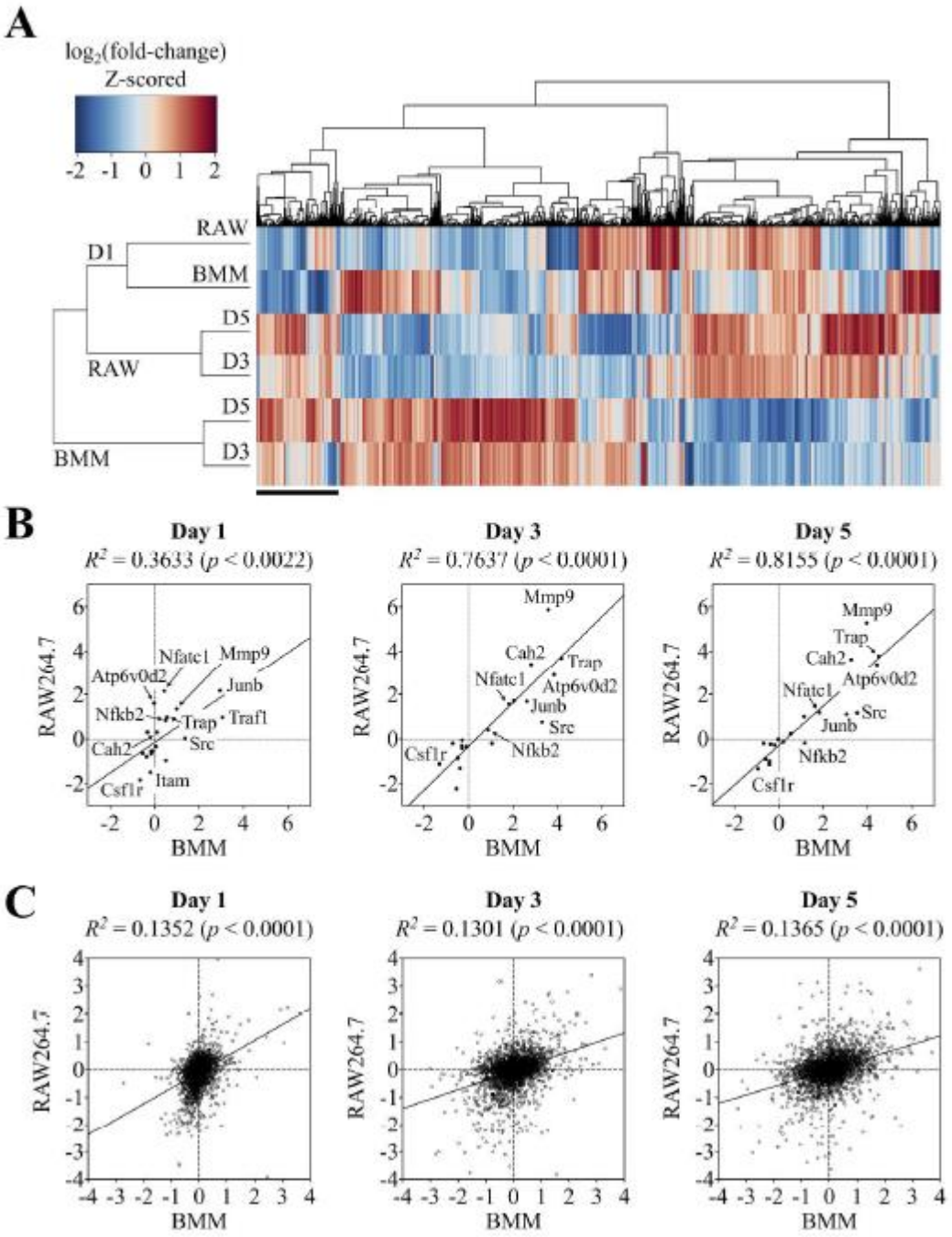

Figure 2

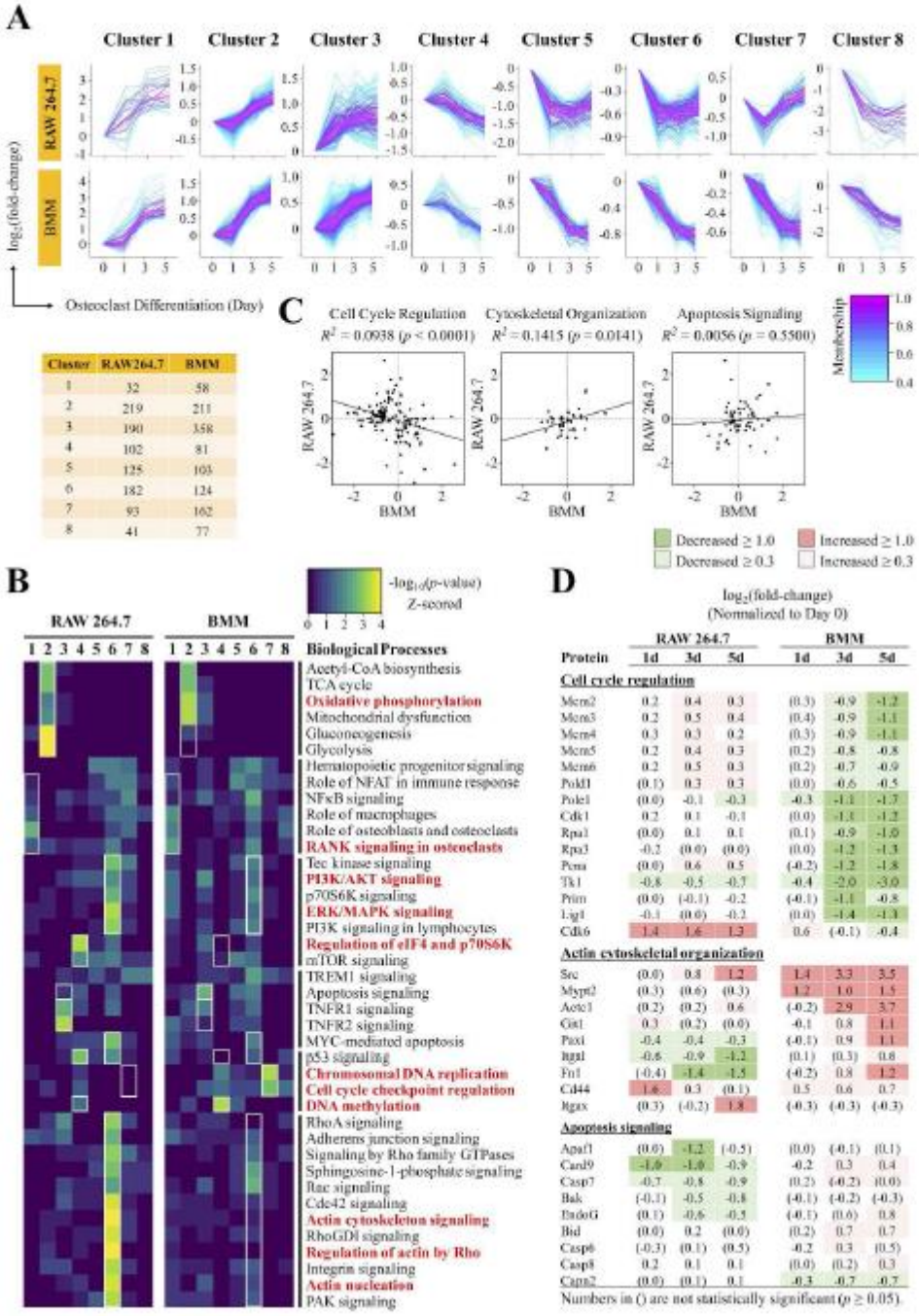

Figure 3

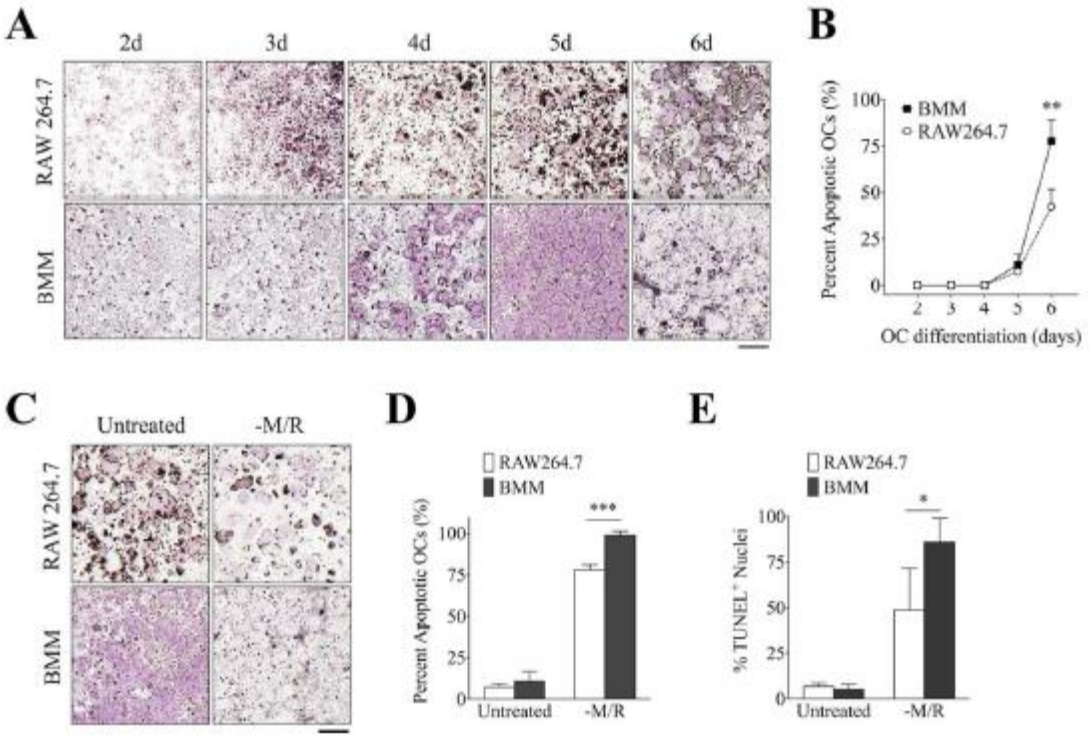

Figure 4

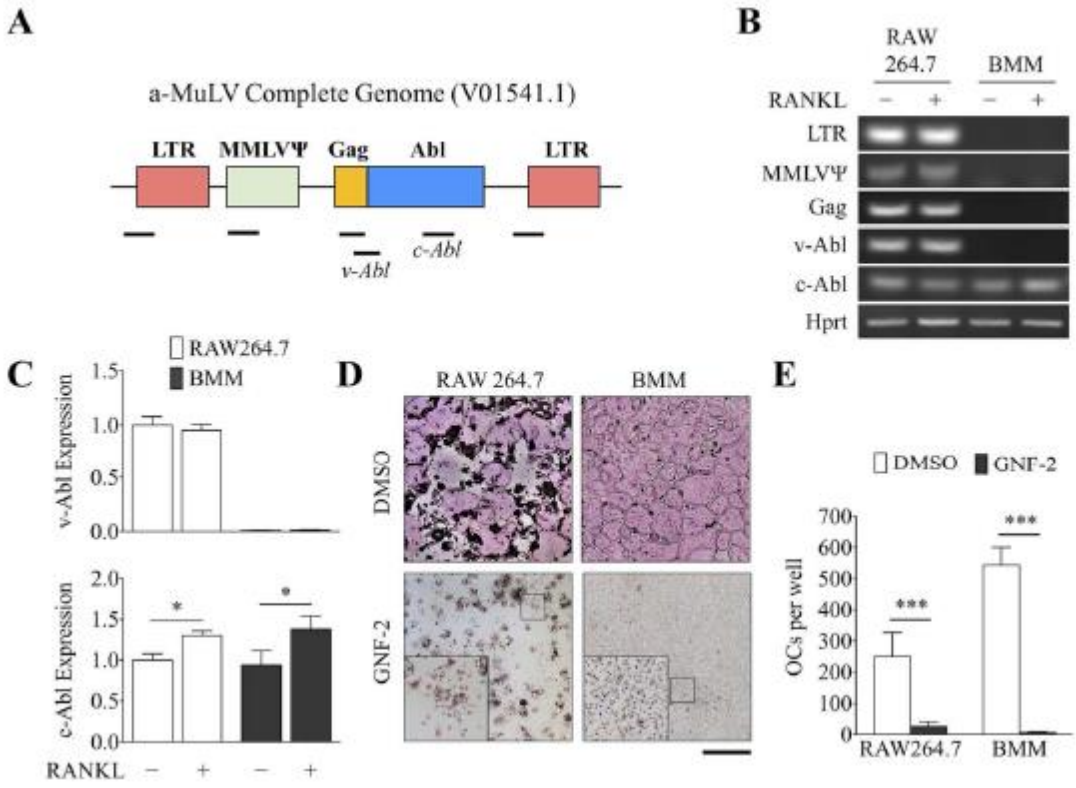

Figure 5

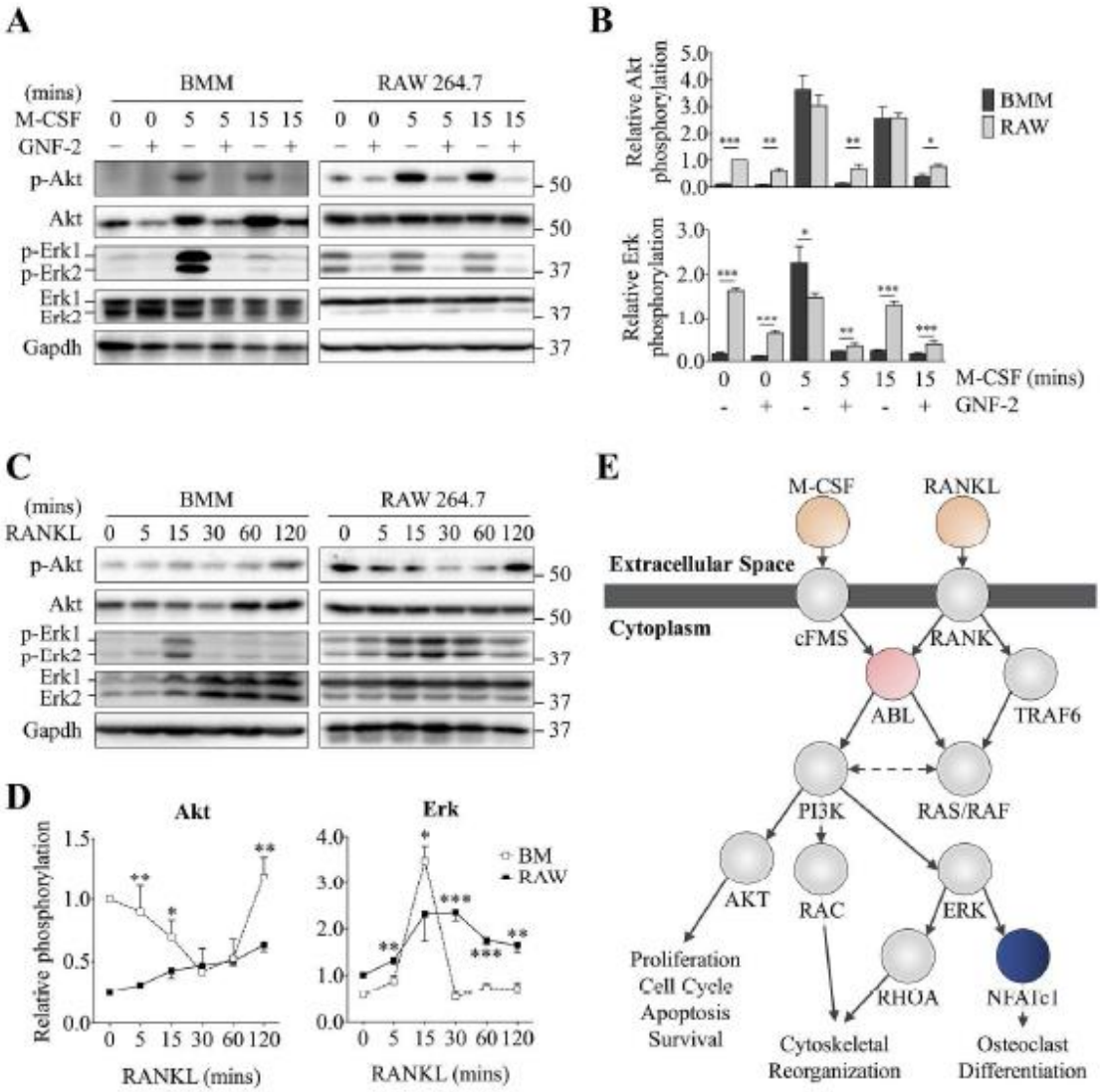

Figure 6